MODEL OF 3D CONJUGATE HEAT TRANSFER AND MECHANISM OF COMPRESSED GAS STORAGE FAILURE IN A FIRE

Kashkarov, S., Makarov, D., Molkov, V.
Hydrogen Safety Engineering and Research Centre (HySAFER), Ulster University, Newtownabbey, BT37 0QB, Northern Ireland, UK, * s.kashkarov@ulster.ac.uk

ABSTRACT

The 3D model of conjugate heat transfer from a fire to compressed gas storage cylinder is described. The model predictions of temperature outside and inside the cylinder as well as pressure increase during a fire are compared against a fire test experiment. The simulation reproduced measured in test temperatures and pressures. The original failure criterion of the cylinder in a fire has been applied in the model. This allowed for the prediction of the cylinder catastrophic rupture time with acceptable engineering accuracy. The significance of 3D modelling is demonstrated, and recommendations to improve safety of high-pressure composite tanks are given.

NOMENCLATURE

A	empirical constant (-), A=4
a	total absorptivity (1/m)/ critical temperature related constant (-)
$a_{\varepsilon,i}$	emissivity weighting factor for i-th grey gas (-)
a_i	partial absorption coefficient (1/m)
B	empirical constant, B=0.5
b	co-volume constant, b = 1.584×10^{-5} (m^3/mol), or b = 7.69×10^{-3} (m^3/kg) /critical pressure related constant (-)
$C_{1\text{-}3\varepsilon}$	empirical constants, $C_{1\varepsilon}$=1.44, $C_{2\varepsilon}$=1.92, $C_{3\varepsilon}$ indicates buoyancy effect on ε (-)
$\bar{c}_{fuel}$	local fuel concentration (kg/m^3)
$\bar{c}_{O2}$	local oxygen concentration (kg/m^3)
$\bar{c}_p$	local products concentration (kg/m^3)
c_p	specific heat (J/kg/K),
D	diffusion coefficient (m^2/s),
E	energy (J),
G_b	generation of turbulence k due to buoyancy, (kg/ms^3)
G_k	generation of turbulence k due to mean velocity gradients (kg/ms^3)
g	gravitational acceleration (m/s^2)
H	enthalpy (J)
H_d	heat of decomposition (J/kg)
I	radiation intensity (W/m^2/sr)
n	index of reflection (-)
k	turbulent kinetic energy (m^2/s^2)/thermal conductivity (W/m/k)
Q	heat flux (W/m^2)
P	pressure (Pa)
p_{tot}	sum of the partial pressures of adsorbing gases (Pa)
R	universal gas constant, R=8.314 (J/mol/K)
R_{fuel}	rate of fuel consumption (kg/m^3/s)
r_{fuel}	stoichiometric oxidizer requirement to combust 1 kg of fuel (-)
$\vec{r}$	vector of location (-)
S	sink term (J/m^3/s)
Sc	Schmidt number (-)
S_m	source term due to combustion (J/m^3/s)
S_k, S_ε	user defined source terms (J/m^3/s)
$\vec{s}'$	direction scattering vector (-)
$\vec{s}$	vector of direction (-)
T	temperature (K)
t	time (s)
u	velocity (m/s)
V	volume (m^3)
x	distance/path length (m)
Y_m	compressibility effect term, (Y_m=2$\rho\varepsilon M_t^2$, where Mach number: M_t=(k/a^2)$^{1/2}$, a - sound speed) (-)

Greek

α	absorptivity (-)
β	decomposition energy fraction (-)
ε	turbulent dissipation rate (m^2/s^3)/ emissivity (-)
Φ	phase function (-)
ρ	density (kg/m^3).
μ_t	turbulence (eddy) viscosity (Pa·s)
σ	Stefan-Boltzmann constant, σ=5.669·10^{-8} (W/m^2-K^4)
σ_ε	turbulent Prandtl constants for ε, σ_ε=1.3 (-)

σ_k	turbulent Prandtl constants for k, σ_k=1 (-)
σ_s	scattering coefficient (1/m)
Φ	phase function (-)
w'	solid angle, $w'=\vec{s}\cdot\vec{r}$ (-)

Subscripts

0	initial/inner
curr	current moment (timestep)
d	decomposition
d_1	lower decomposition threshold
d_2	upper decomposition threshold
f	final
fuel	fuel
g	gas
i, j,k	direction
NWP	nominal working pressure
tot	total

Abbreviations

CFD	computational fluid dynamics
CFRP	carbon fibre reinforced polymer
CGH2	compressed gaseous hydrogen
COPV	composite overwrapped pressure vessel
GTR	Global Technical Regulation
HDPE	high density polyethylene
HGV	heavy goods vehicle
HPV	hydroge-powered vehicle
HRR	heat release rates
LDV	light duty vehicle
NWP	nominal working pressure
PRD	pressure relief device
RCS	regulations, codes and standards
SUV	sports utility vehicle
TGA	thermogravimetric analysis
TPRD	thermally activated pressure relief device
WSGG	weighted sum of grey gases model.

1.0 INTRODUCTION

The exploitation of compressed gaseous hydrogen (CGH2) as a "green" fuel is beneficial for the environment. Though, there also are safety issues. The safety aspects of the hydrogen storage systems exploitation have been carefully investigated by the hydrogen safety community during the recent years. The storage system includes but is not limited to a pressurised gas storage tank and pressure relief device. Type IV tanks are typically accepted as onboard CGH2 storage for their exceptional weight and strength characteristics. Though these composite overwrapped pressure vessels (COPV) have good mechanical performance, they tend to degrage under thermal load and have a high failure risk under accidental fire exposure. Moreover, fire resistance rating (FRR) of COPV with carbon-fibre reinforced polymer (CFRP) jackets is currently unacceptably low. There are known catastrophic accidents, where storage vessles exploded due to the pressure relief devices (PRD) failures to operate [1]–[5]. The recent USA fire tests with hydrogen tanks not equipped with PRD were performed with HRRs 370 kW and 265 kW giving times to tanks rupture 6.5 and 12 min; the FRR of Type IV tank in recent experiment (presented in the study) totalled 8 min. The studied economic effect from the current state-of-the-art of safety of hydrogen storage [6] showed the cost associated with such a low FRR (i.e. 8 min) wich is £2M per accident. Also the hazardous consequences, i.e. (blast wave and fireball) from a high-pressure hydrogen tank rupture, are currently horoughly studied [7]–[10].

The statistics on fires occurred in hydrogen-powered vehicles (HPV) is absent up to date. Nevertheless, as the hydrogen infrastructure develops in different countries, the HPV fleet also grows accordingly. This implies, that vehicles with compressed gas storage vessels onboard are subject to risk of fires as much as gasoline vehicles.

The following review of statistics of vehicle fires and experimentally measured heat release rates extracted from related tests will feed the necessity of research performed in current paper. The average annual number of car fires in Great Britain was about 64,100 from 2000 to 2012 yy [11]. The average annual number of vehicle fires in the USA from 2003 to 2007 yy was 287,000 [12]. At the USA service stations from 2004-2008 yy the vehicle fires comprised [13]. In Great Britain, for the period since 1994 to 2005 (12 years) it was registered 3096 car park fires (in buildings); nearly half, i.e. 1592, initiated in vehicles [14]. Such figures give an idea that fires shall affect compressed gas storage leading to rupture and jeopardising life and property safety.

The detailed insight into the specificities of a fire test with a compressed gas storage tank and estimation of time to failure is possible with numerical computational fluid dynamics (CFD) investigation. The review of existing models for compressed gas tank response to a fire revealed some drawbacks that the developed model aims to fix.

The model [15] realised the heat flux input to the tank as adoption of the solution of 3D tank behaviour in CFD fire test simulations with radiation. From these 3D simulations, the mean heat fluxes on tank wall of its side and bottom positions were applied as constant in time for 2D finite element model. This was done for speeding up calculations, as authors claimed the 3D simulations of the experiment, i.e. 6 min 27 s [16], is "beyond the capability of our available computing resources" [15]. The simplified failure criterion suggested by authors is based on the grown internal tank pressure due to temperature increase until the pressure becomes equal to the experimental rupture pressure. In experiment [16] the stored hydrogen pressure grew from initial 34.3 MPa to final 35.7 MPa (when rupture occurred). The equation $P = 1.2T + 320$ was implemented in the model to predict the pressure dynamics [15]. The model predicted time to failure 6 min 39 s (when internal pressure raised to 35.7 MPa). The experimental value iss 6 min 27 s [16]. It is obvious that the pressure prediction is described by a temperature function and does not implement a real gas law.

Another model [17] also implemented finite element approach using axisymmetric problem. The flame aggression to the tank was modelled through constant heat flux on its surface, "the radiation, as well as the convection, is also considered at the cylinder outside surface" [17].

The model by Zheng et al [18]–[20] applied for engulfing and localised fire tests. The model included RNG turbulence model and Eddy-Dissipation model for combustion of non-premixed turbulent flames and did not include radiation model.

The model developed during the FireComp project [21] assumed the constant heat flux over time that was applied on the tank. The tank was modelled as 2D axisymmetric simplification. The time to failure of the tank in the simulation was assessed through analysis of failure of one of hoop layers.

Thermal response of COPV to a fire was studied by different authors [22]–[26]. The extensive experimental study presented in [27] highlighted the importance of understanding of a failure mechanism as "identifying the main failure mechanism is key to optimising the fire protection means implemented in Type IV pressure vessels". The outcomes from the tests were ruptures of two vessels (pressurised at 70 and 52.5 MPa) and leakages of the other two (pressurised at 35 and 17.5 MPa). The experimental analysis provided measurements of temperatures inside composite. In the context of one of the vessels that leaked, the measured temperature inbetween CFRP and liner in cylindrical part of the vessel did not reach the liner melting temperature. However, in junction between dome and cylindrical parts of the vessel indicated temperature 573 K, i.e. higher than liner melting temperature (488 K). These experimental observations even more underpin the importance of 3D modelling and analysis that should provide a better insight into the tank behaviour in a fire.

The aim of this study is to develop and validate 3D numerical model of conjugate heat transfer to compressed gas vessel from a fire including the failure mechanism for such a vessel. The model should eliminate the drawbacks identified in the above models and account for: full scale 3D fire source combustion including radiation; non-uniform, 3-dimensional and time dependant thermal load on the tank; the real gas behaviour of hydrogen and pressure load-dependant criterion for COPV failure in a fire including composite structural layer degradation.

2.0 VALIDATION EXPERIMENT

The fire test experiment was conducted at Karlsruhe Institute of Technology (KIT) (Germany). The experimental facility was HyKA-A2, which represents a vessel (V=220 m^3) designed to withstand 10 bar of static overpressure. The fire source and the hydrogen tank with all the instrumentation were installed inside the facility. During the fire test experiment the A2 facility was perfectly sealed, not allowing for products to escape. The experiment was conducted with 36 L Type IV (supplied by

Hexagon Composites) tank filled with hydrogen gas at initial nominal working pressure (NWP) ~700 bar. Because the tank rupture in a fire was the intended test otcome, to avoid combustion of hydrogen gas released after tank failure, the ambient gas inside the A2 facility was nitrogen. The fuel in this fire tests was methane which was released in a mixture with air. The mixing ratio was 10:1 of air to $CH4$ by volume. The mixture was prior-formed in chambers located underneath the burner plates. 5 thermocouples (TCs) located above the tank (TX, T06-T09) and 5 TCs located aside the fire source at a distance ~2 m (T01-T05) measured products temperatures. Three thermocouples (BL000, BM000, BR000) were suspended under the tank bottom at distance 25 mm to measure the flame temperatures, in accordance with GTR No. 13 [28]. The steel caps were utilised to cover thermocouples for the purpose of smoothing the temperature history oscillations. Figure 1 schematically shows the facility with TCs locations and hydrogen tank positioned over the fire source installation with TCs suspended underneath.

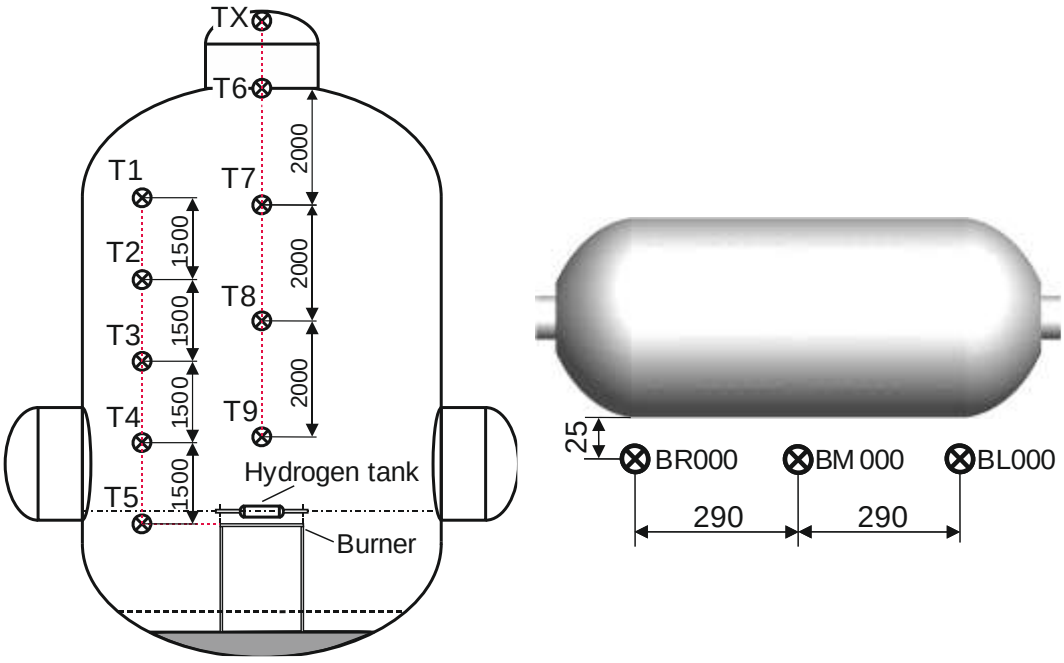

Figure 1. Schematic views of experimental HyKA A2 facility and thermocouples locations [29] (left) and schematic view of location of TCs BL000, BM000 and BR000 under tank (right).

Flame arresters (burner plates) were utilised in the fire source design in order to prevent the flame from burning back into the mixing chambers and fuel supplying lines. These are the sintered metal plates made from porous material with narrow channels. The fire source comprised three of such burner plates. These burners were encompassed into the metal frame. Another specificity of the fire source was that it had the shields, i.e. guide plates, that helped to direct the flame distribution to the tank. The hydrogen tank fittings with the bosses and the filling line were placed into insulating pipes with an inner diameter of 10 cm. This is in line with GTR No. 13: "metallic shielding is used to prevent direct flame impingement on container valves, fittings, and/or pressure relief devices" [28]. Insulation pipes extended up to 0.38 m above the fire source and beyond it to cover and protect the filling line so that its region subjected to a fire is insulated. The fire source including the casing frame, guide plates and three burners (1-3) are shown in Figure 2.

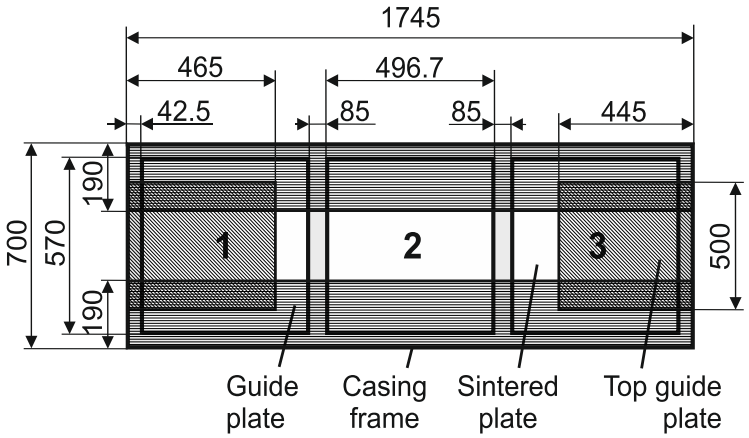

Figure 2. The scheme of the fire source including burners 1-3 [30] with dimensions (top view).

The mean mass flow rate of CH4-air mixture set for the fire source in the 165 kW test was 59 g/s. The initial pressure and temperature inside the test facility and hydrogen tank per each experiment are given in Table 1.

Table 1. Initial pressures and temperatures in hydrogen tank and experimental facility.

Test HRR	Tank initial conditions		Facility initial conditions	
	P, Pa	T, K	P, Pa	T, K
165 kW	70,095,633.4	308.095	7,312.2	294.33

3.0 THE MODEL

3.1. Physical model

GTR No. 13 [28] requires that the tank integrity is tested when it is pressurised up to 225% of nominal working pressure (NWP). This is the safety factor for CFRP overwrapped (Type IV) tanks. Therefore, under NWP the fraction of a CFRP structural wall thickness fraction capable of bearing the load is 100%/225%=0.44(4). The fraction of the CFRP wall thickness 1-0.44(4)=0.55(5) represents the safety margin. This safety margin may tend to decrease as the load-bearing fraction (0.44) grows.

If the tank is subject to a fire and the composite structural jacket is heated over the time, the epoxy resin (binder) shall tend to degrade (characterised by a substantial mass loss). The structural integrity of a cylinder due to thermal agression gets lost when the resin decomposes and neighbouring fibre plies in composite become not bound together. When in a fire, the tank's internal pressure starts to grow above a NWP due to the hydrogen gas heating and, therefore, safety margin fraction starts to decrease as 1-[(P_{curr} / 2.25) / P_{NWP}]. Here P_{curr} is the current pressure and P_{NWP} is the nominal working pressure. The tank failure in a fire mechanism postulates that the tank stops holding the compressed gas inside when the safety margin fraction is consumed by decomposition wave in the CFRP. It should be noted that the significance of role of the safety factor for CFRP cylinders (225% [28]) was not pronounced in the reviewed in this study models.

The decomposition of carbon fibre is not considered in the study because the fire test ambient gas inside the testing facility was not oxidative, i.e. nitrogen. Only the epoxy resin decomposition was accounted for the failure mechanism. This assumption is supported by experimental TGA observations discussed in the relevant paper [27]. It was demonstrated that "with an inert atmosphere, the sample displayed only one decomposition stage (from 493 K to 773 K). This corresponds to the decomposition of epoxy resin". The decomposition (mass loss) of the tested in the paper [27] specimen at temperatures above 873 K (typical for carbon fibre) was absent.

3.2. Mathematical model

3.2.1. Governing equations

Mass, momentum, energy and species conservation equations

The mass conservation equation is written as:

$$\frac{\partial \bar{\rho}}{\partial t} + \frac{\partial}{\partial x_j}(\bar{\rho}\tilde{u}_j) = 0. \qquad (1)$$

Momentum conservation is:

$$\frac{\partial \bar{\rho}\tilde{u}_i}{\partial t} + \frac{\partial}{\partial x_j}\left(\bar{\rho}\tilde{u}_j\tilde{u}_i\right) = -\frac{\partial \bar{P}}{\partial x_i} + \frac{\partial}{\partial x_j}\left(\mu + \mu_t\right)\left(\frac{\partial \tilde{u}_i}{\partial x_j} + \frac{\partial \tilde{u}_j}{\partial x_i} - \frac{2}{3}\frac{\partial \tilde{u}_k}{\partial x_k}\delta_{ij}\right) + \bar{\rho}g_i. \qquad (2)$$

The energy conservation equation is given as:

$$\frac{\partial}{\partial t}\left(\bar{\rho}\tilde{E}\right) + \frac{\partial}{\partial x_j}\left(\tilde{u}_j\left(\bar{\rho}\tilde{E} + \bar{P}\right)\right) =$$

$$= \frac{\partial}{\partial x_j}\left(\left(k + \frac{\mu_t c_p}{Pr_t}\right)\frac{\partial \tilde{T}}{\partial x_j} - \sum_m \tilde{h}_m\left(-\left(\rho D + \frac{\mu_t}{Sc_t}\right)\frac{\partial \tilde{Y}_m}{\partial x_j}\right) + \tilde{u}_i\left(\mu + \mu_t\right)\left(\frac{\partial \tilde{u}_i}{\partial x_j} + \frac{\partial \tilde{u}_j}{\partial x_i} - \frac{2}{3}\frac{\partial \tilde{u}_k}{\partial x_k}\delta_{ij}\right)\right) + S_E, \qquad (3)$$

where S_E is the source term.

The species transport equation is written in a form:

$$\frac{\partial \bar{\rho}\tilde{Y}_m}{\partial t} + \frac{\partial}{\partial x_j}\left(\bar{\rho}\tilde{u}_j\tilde{Y}_m\right) = \frac{\partial}{\partial x_j}\left(\left(\rho D + \frac{\mu_t}{Sc_t}\right)\frac{\partial \tilde{Y}_m}{\partial x_j}\right) + S_m, \qquad (4)$$

where S_m is the source term due to combustion.

Turbulence model

The standard $k-\varepsilon$ model [31] with standard wall functions was used in simulations. This two-equation model describes transport for kinetic energy, k, and dissipation rate, ε, as:

$$\frac{\partial}{\partial t}(\rho k) + \frac{\partial}{\partial x_i}(\rho k u_i) = \frac{\partial}{\partial x_j}\left[\left(\mu + \frac{\mu_t}{\sigma_k}\right)\frac{\partial k}{\partial x_j}\right] + G_k + G_b - \rho\varepsilon - Y_m + S_k \qquad (5)$$

and

$$\frac{\partial}{\partial t}(\rho\varepsilon) + \frac{\partial}{\partial x_i}(\rho\varepsilon u_i) = \frac{\partial}{\partial x_j}\left[\left(\mu + \frac{\mu_t}{\sigma_\varepsilon}\right)\frac{\partial \varepsilon}{\partial x_j}\right] + C_{1\varepsilon}\frac{\varepsilon}{k}\left(G_k + C_{3\varepsilon}G_b\right) - C_{2\varepsilon}\rho\frac{\varepsilon^2}{k} + S_\varepsilon. \qquad (6)$$

Combustion model

According to the used in this CFD model "Eddy-Dissipation", as introduced by Magnussen and Hjertager [32], the rate of combustion is determined in general form as:

$$R_{fuel} = A \cdot \left(\frac{\varepsilon}{k}\right) \min\left\{\bar{c}_{fuel}\left(\bar{c}_{O2}/r_{fuel}\right), B \cdot \bar{c}_p\left(1 + r_{fuel}\right)\right\}. \quad (7)$$

Radiation model

The Discrete Ordinates (DO) [33], [34] radiation model was utilised in the model. It suits well for combustion problems and covers the entire range of the flame optical thicknesses. The radiative transfer equation is [33], [35]:

$$\frac{dI(\vec{r},\vec{s})}{dx} = -(a_i + \sigma_s)I(\vec{r},\vec{s}) + a_i I(\vec{r}) + \sigma_s \bar{I}(\vec{r},\vec{s}). \quad (8)$$

On the right hand side of the equation above, the term $(a_i + \sigma_s)I(\vec{r},\vec{s})$ is the absorption; the second term is the emissivity term; the last term in the right hand-side is the scattering.

Absorptivity in the gas media, where the combustion products, CO_2 and H_2O, are present, was calculated using Weighted Sum of Grey Gases model (WSGGM). It was presented by [36], later also published in [37] and is widely used in CFD modelling of combustion problems for gas media. FLUENT [38] calculates the total gas media absorptivity as: $\alpha = -[\ln(1-\varepsilon)]/s$. Here emissivity, ε, is :

$$\varepsilon = \sum_{i=0}^{I} a_{\varepsilon,i}\left(T_g\right)\left(1 - e^{-a_i \cdot p_{tot} \cdot x}\right), \quad (9)$$

where term $a_{\varepsilon,i}(T_g)$ is the temperature dependent emissivity weighting factor for i-th grey gas and term 1-$e^{-a_i \cdot p_{tot} \cdot x}$ is the emissivity of the i-th grey gas.

Real gas

The hydrogen gas was specified as a real gas in CFD model. The chosen model for the real gas was Redlich-Kwong. The equation of state [39] is written as:

$$P_{curr} = \frac{RT}{V-b} - \frac{a}{V(V+b)T^{0.5}}, \quad (10)$$

where V is the specific molar volume, a and b are the constant related to critical temperature and pressure.

Composite degradation

The decomposition of resin in CFRP is realised in CFD model through the user defined function (UDF). The modelling of this process involves the sink term in energy equation. The term calculates the loss of energy, i.e. energy spenditure on decomposition, only when the defined decomposition temperature range (thresholding the decomposition wave) is attained in a control volume of the CFRP solid body.

The decomposition is driven by the fraction, β, which complies with the following temperature-related conditions. Firstly, there is no decomposition (β=0) if the current control volume temperature, T_{curr}, is below the lower chosen decomposition temperature threshold, T_{d1}, or reached the value above the upper chosen decomposition temperature threshold, T_{d2}. Decomposition applies (β=1) if the current control volume temperature is within the selected range of decomposition temperatures (T_{d1} and T_{d2}), i.e.

$T_{curr} \geq T_{d1}$ and $T_{curr} \leq T_{d2}$. Thus, the failure mechanism is based not on a single decomposition temperature, but on a range of temperatures, from T_{d1} to T_{d2}. The energy equation for a solid body is written in a form:

$$\rho \frac{\partial}{\partial t} H = \nabla \cdot (k \nabla T) + S \,. \tag{11}$$

The 1st term on the right hand side of equation means the heat flux due to conduction. The last term, S, (originally the heat sourse in the energy equation) is implied for the energy sink in the model due to decomposition and is calculated as $S = -\rho \cdot \beta \cdot \partial H_d / \partial t$. The energy value, H_d, grows as the fraction β increases from 0 to 1, in accordance to the conditions described above.

4.0 NUMERICAL DETAILS

4.1. Calculation domain and numerical mesh

Numerical mesh of the calculation domain consists of hydrogen "gas" cell zone, hydrogen tank cell zone and ambient "gas" cell zone (facility). The numerical mesh for hydrogen gas mesh and ambient gas, including fire source with installation, is designed using tetrahedral mesh. Tetra cells were converted to polyhedral cells in ANSYS FLUENT solver. The mesh of Type IV tank was designed using hexahedral mesh. The geometry of the tank was supplied by Hexagon Composites [40]. The CFRP wall thickness in the tank was resolved by 29 hexahedral control volumes. This results in control volume size ~0.95 mm for cylindrical part and ~0.75 mm for the thinner dome part. The numbers of control volumes totalled 939.8k for domain. Figure 3 (left) shows outside 3D view of the HyKA A2 test facility (calculation domain) and Figure 3 (right) shows the burner installation with flame shielding, insulation pipes and installed hydrogen tank.

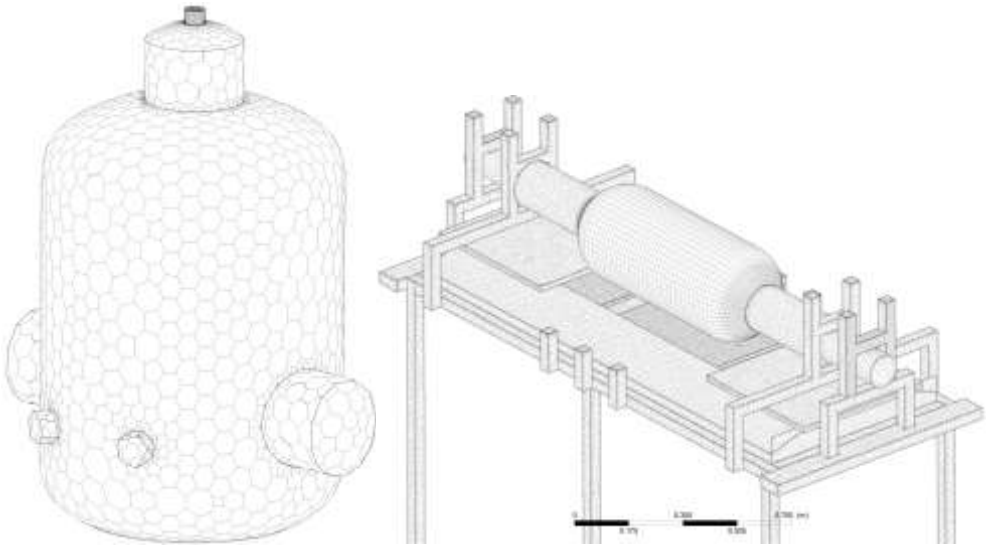

Figure 3. Numerical mesh of testing facility (left) and premixed burner installation with positioned hydrogen tank (right).

The steel "cubes" implemented in the experiments for smothering temperatures oscillations were modelled in the simulations as the cubic solid bodies with the steel material properties.

4.2. Initial and boundary conditions

The meshes of hydrogen gas, tank and facility (ambience) were designed separately and then composed into the consistent system. Therefore, these meshes were non-conformal to each other. To resolve this, the ANSYS FLUENT feature Mesh Interfaces was applied for fluid/solid regions of the mesh, where

two unconformal adjacent cells' faces are coupled together (in this case "the solver will calculate heat transfer directly from the solution in the adjacent cells" [38]). The conjugate heat transfer to the A2 facility metal wall was modelled including conduction inside the wall calculated by solving 1D steady conduction equation. This simplification was achieved through FLUENT [38] feature; the wall thickness 26 cm was specified, as per facility specifications. The emissivity properties on the surfaces boundary conditions of objects were specified as follows: hydrogen tank (carbon fibre polymer/carbon) ε=0.91 [41]; thermocouple caps (steel) ε=0.5 [42], [43].

4.3. Material properties of fydrogen tanks components

The Type IV COPV components are: CFRP structural layer (jacket), HDPE non-structural and non-permeable liner and two aluminium bosses. The thermo-physical properties of these components were reviewed and the review is summarised in Table 2 below.

Table 2. Thermo-physical properties of cylinder components.

Component	k, W/m/K	ρ, kg/m3	c_p, J/kg/K	Reference
Bosses (aluminium)	202.4*	2719*	871*	[38]
	218	2700	902	[20]
Cylinder jacket (CFRP)	0.25 ~ 1.0	-	-	[44]
	0.304+8.52×10-4T	1750	-19+3T	[19]
	0.4 ~ 0.8	-	-	[45]
	0.43 ~ 0.5	-	-	[46]
	0.48 ± 0.05	1472 ± 20	900	[47]
	0.5	1360*	1020*	[48]
	0.5 ~ 0.61	-	-	[49]
	0.5 ~ 0.8	-	-	[50]
	0.6 ± 0.3	-	-	[51]
	0.65	-	897.79791+2.9932T	[17]
	0.67	1530	950	[52]
	0.71	-	-	[45], [53]
	0.74	1494	1120	[54]
	0.99710-8×10-4· T	1588.39-0.0425T	685.750+1.3933T	[55]
	1 ~ 1.3	-	-	[56]
	1.32**	-	-	[57] **
	2.9	1760	800	[58]
	3.72	1513	920	[59]
	6.5	1750	-19+3T	[20]
Liner, (HDPE)	0.4(@293 K)-0.2(@423 K)*	940*	2000(@293 K)-2600(@423 K)*	[60]
	0.385	945	1584	[54]
	0.45	960	2250	[15], [61]

Note: * is the thermophysical properties of the hydrogen tank components used in the model; ** is the thermal conductivity measured during this study.

Composite degradation parameters

The review of decomposition temperatures of the polymer resins identified that these temperatures scatter. The most common range of temperatures at which resins start to decompose is 300-400°C (573-673 K). These temperatures can be as low as 319°C (10% mass loss) [62]. Other authors, i.e. [63] and [52] stated the temperatures are 350°C and 360°C respectively. [64] provided an experimental data on epoxy/carbon decomposition temperature within 296-366°C (the second decomposition step step varied 452-559°C). Other epoxy resins can have thermal degradation temperature as high as 440°C [65]. Niranjana Prabhu [66] gave temperatures for the epoxy resins in composites ranging 280-375°C. Liu et

al in the same publication [62] have shown the decomposition temperature 379°C. Chiang et al [67] provided the value 375°C. The performed thermogravimetric analysis [68] showed decomposition temperatures of 340-360°C (613-633 K), which is found to be within the range of temperatues available in literature. The simulations represented in current work involved the ranges of decomposition temperatures of 370°-379°C (643-652 K), as per [64] and [67].

The decomposition heat values may vary significantly. The work by [55] provides the value of 1.92 MJ/kg (as calculated in [69]). Another source [17] gives the heat of decomposition of the resin 0.35 MJ/kg. The authors implemented the latter value of decomposition heat for the failure mechanism .

5.0 RESULTS AND DISCUSSION

5.1. Temperature and pressure histories

The pressure histories monitored during the simulation inside the testing facility and hydrogen tank were recorded every second. The comparison of pressures in the A2 facility and in the tank between experiment and 3D simulation is given in Figure 4.

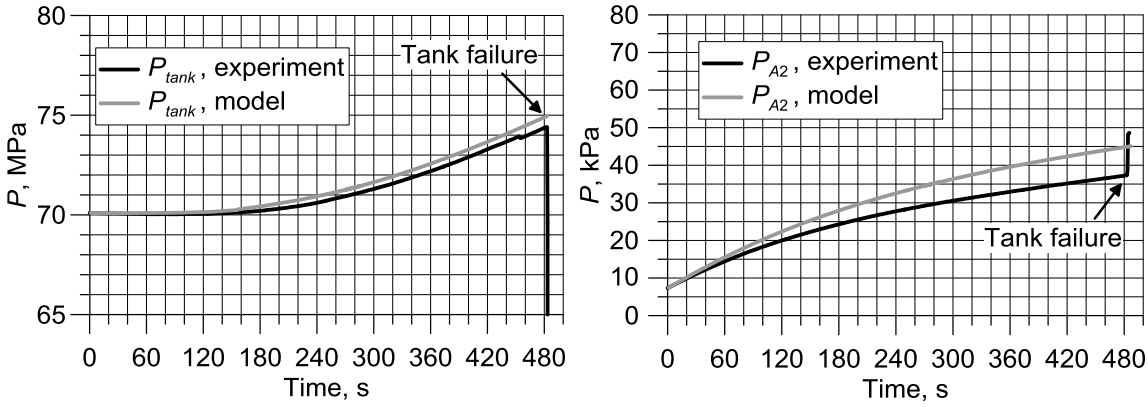

Figure 4. Comparison of pressures dynamics inside the tank (left) and inside A2 facility (right): simulations compared with experimental and identified time of tank failure (483 s).

The model predicted the hydrogen tank internal pressure dynamics (Figure 4, left) with the maximum over-estimation about 1% but the model over-predicted experimental pressure inside the testing facility by 20%.

The temperatures of the flame were monitored in steel cubes located under the tank bottom, as per experimental arrangements described in Figure 1 of section “Validation experiment”. The comparison of temperatures under the tank in experiment and 3D simulation is given in Figure 5.

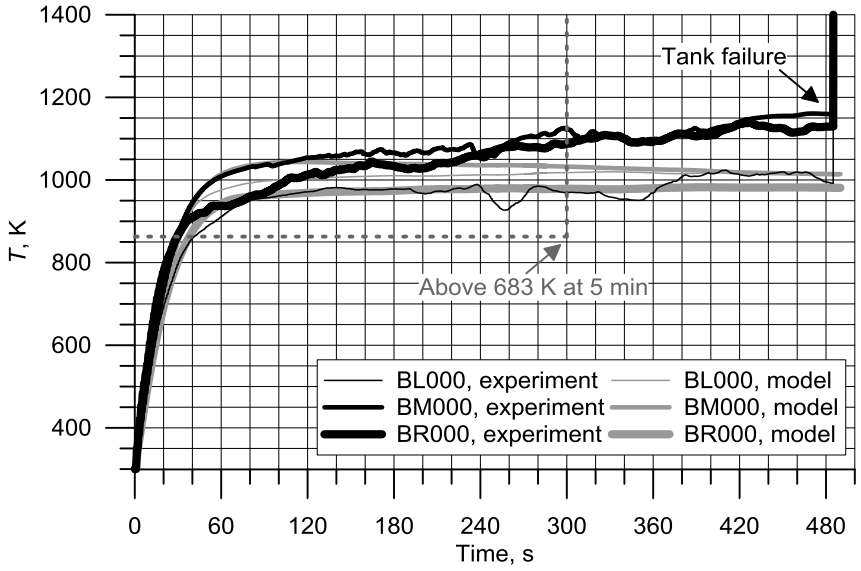

Figure 5. Temperature histories in TCs BL000, BM000 and BR000 at 25 mm under the tank: comparison of model results with experimental data and identified fulfillment of minimum temperature requirement from GTR No. 13 (683 K).

It can be seen from Figure 5 that simulated temperatures in TCs suspended under the tank have the maximum deviation from experimental temperatures in the end of the test – 12 % under-prediction for TC BM000 and almost 4% for TC BR000.

The vertically arranged TCs inside the testing facility measured temperatures throughout the test duration. The temperatures of interior of the testing facility were monitored in the 3D model corresponding to locations of TCs positioned in the experiment. Predictions of temperatures measured by TCs located vertically above the tank (T6-T9 and TX) and 2 m aside from the tank (T1-T5), are shown in Figure 6 and Figure 7 below.

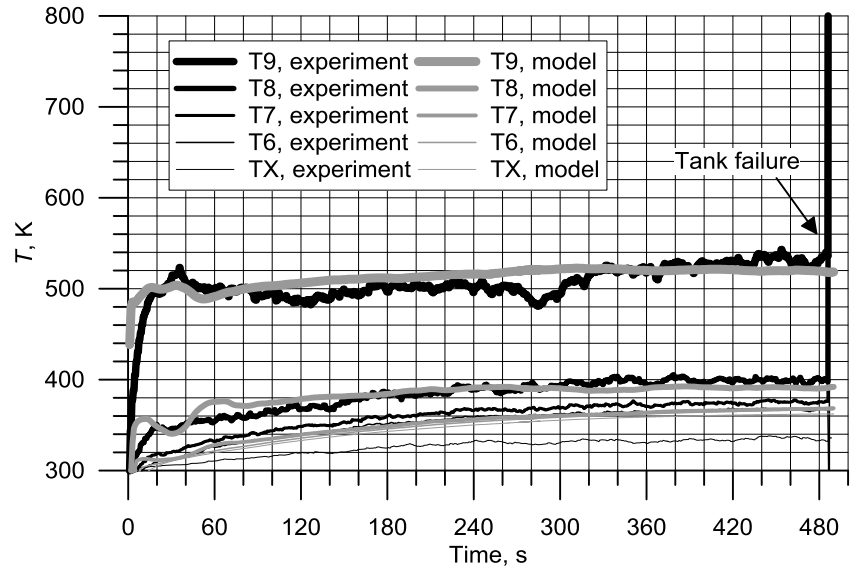

Figure 6. Temperature histories in vertically located TCs T6-T9 and TX above the tank: comparison of model results with experimental data.

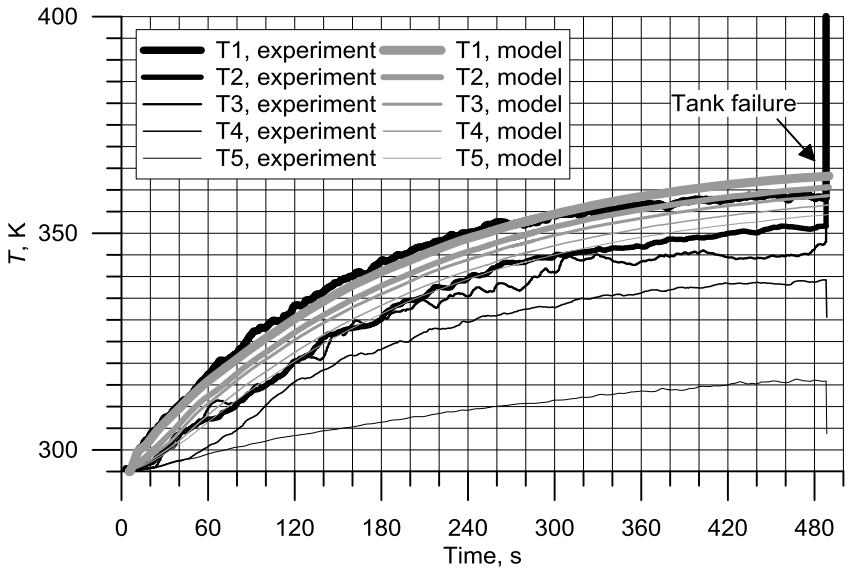

Figure 7. Temperature histories in vertically located TCs T1-T5 at the distance 2 m aside from the tank: comparison of model results with experimental data.

It is shown in Figure 6 that TCs T8 and T9 are in a very good agreement with the experiment. It is worth noting that these temperatures are more representative (as well as temperatures under the tank) as they testify the accuracy of the fire test behaviour near the tank. Temperatures in TCs T7 and TX deviate from experiment by 2% over-prediction for T7 (maximum) and 8% under-prediction respectively. The bigger deviations from experimental temperatures were obtained for TCs located vertically at distance 2 m from the tank, expecially in TCs T2-T5. The biggest over-predictions are: 3% (T2), 3% (T3), 5% (T4) and 12% (T5).

The temperatures evolution inside the testing facility limited by temperature 600 K (for the better dynamics visualisation) is shown in Figure 8.

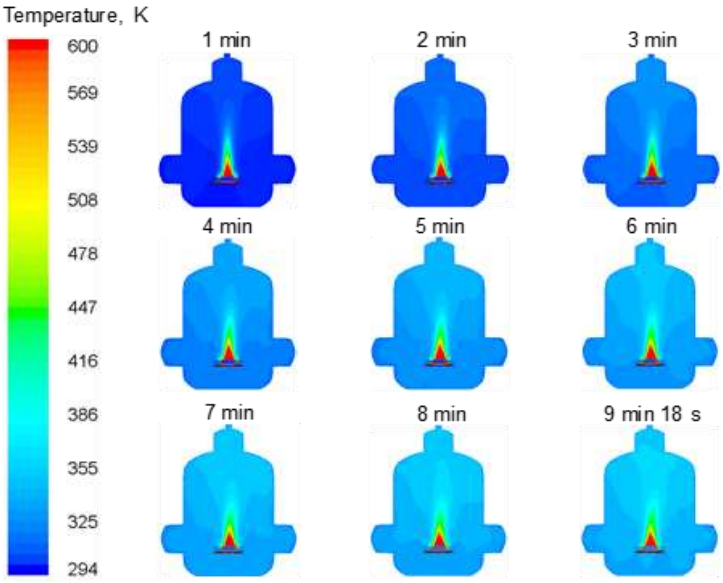

Figure 8. Temperature evolution (limited within the range 294-600 K) inside the A2 testing facility within the simulated fire test duration – A2 middle cross-section, front view.

The temperatures field in Figure 8 was limited by 600 K for the better visualisation of the hot products dynamics in the testing vessel. The maximum temperature in the domain reached ~1850 K. The temperatures above 600 K are also shown in red colour.

5.2. Gas storage tank failure in a fire

The time to failure of the tank in a fire is identified in 3D model as follows. When the decomposition wave (limited by the temperatures 643-652 K, i.e. 370-379ºC) propagated in depth of the CFRP structural layer and came in contact with the virtual load bearing thickness of this layer, the vessel is assumed to fail holding internal pressure and rupture in the place of this contact. According to the failure mechanism, the load bearing thickness of CFRP layer changes dynamically, i.e. it shall expand as the internal tank pressure grows and therefore more thickness of the structural layer shall be needed to hold the higher pressure. Figure 9 shows the visualisation of the identified failure location in the CFRP at the moment when the lower temperature of decomposition from the given decomposition wave range 643-652 K (shown as red iso-surface), contacts with the load-bearing wall fraction (shown as green iso-surface); the bosses (shown in grey colour) are given for the completeness of the tank components.

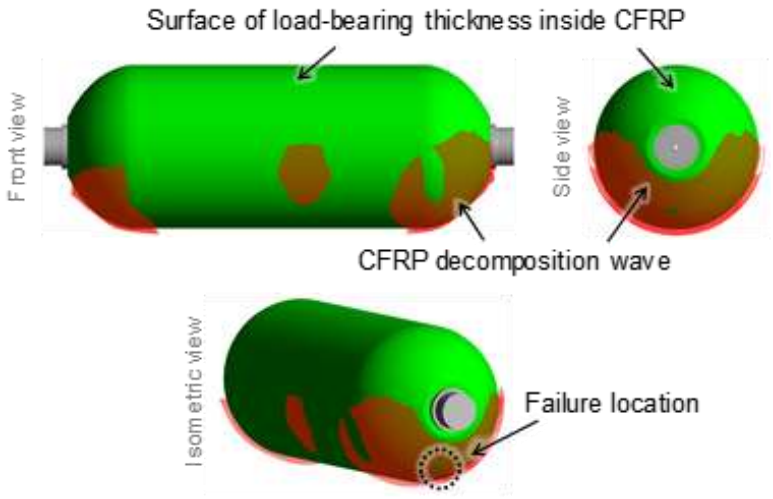

Figure 9. Visualisation of CFRP load-bering thickness surface (green) inside the jacket, decomposition wave iso-surface (red) and identified location where they came in contact at 9 min 18 s.

It is seen in Figure 9 (front view, upper left) that decomposition wave (red transparent surfaces) approached the load-bearing thickness (green surface) nearest closest in dome parts. The decomposition wave is almost missing in the cylindrical part of the tank, especially on the bottom. This is deemed to occur due to the specific burner and flame shielding design as the lower flame temperatures were near the cylindrical part (above the middle burner). The top guide plates (plates horizontally placed above the first and the third burners, as shown in Figure 2) directed the flame and hot products emanating from the side (first and third) burners towards the domes. After analysis of temperatures on dome and cylindrical parts of the tank, the found CFRP surface temperatures grew up to ~812 K and ~545 K respectively (i.e. 49%) by the time 9 min 18 s (predicted by model time of rupture). Also, the CFRP wall in the tank dome part is thinner than that of the cylindrical part by ~27%. Therefore, the decomposition wave approaches the load-bearing thickness in dome part faster, than in the cylindrical part (because it is thicker).

To precisely detect the time to failure of the tank, the temperature on the load-bearing thickness “face” was constantly recorded at each second, i.e. it was monitored when moving towards the approaching decomposition wave travelling from the opposite direction, i.e. from the jacket outer surface subject to a fire. When the decomposition wave lower temperature, i.e. 643 K, was attained on the dynamically moving “face”, the decomposition process has initiated in accordance to the decomposition model. Then, the representative thickness turned unable to hold the increased by that time pressure and the

vessel failed. Figure 10 depicts the temperature growth on the expanding load bearing thickness inside CFRP jacket over the test duration and the identified time of failure.

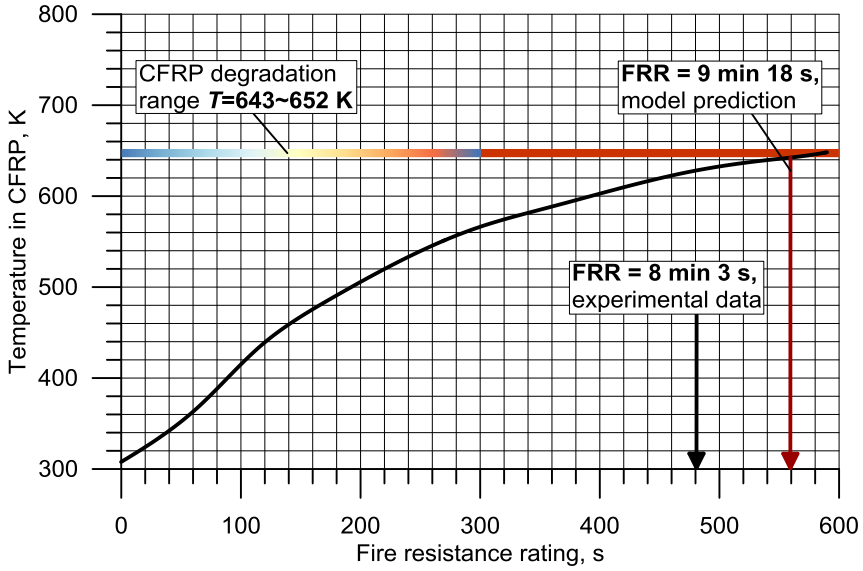

Figure 10. Visualisation of temperature history on the dynamically changing load bearing thickness of the tank CFRP jacket and its coincidence with decomposition wave temperatures 643-652 K.

The given above in Figure 10 temperature history inside the composite tank wall for the numerical test shows the identified time to failure of the tank, i.e. FRR. The deviation of FRR predicted by model from the experimentally documented FRR is shown in Table 3.

Table 3. Comparison of the tank FRR predicted by model and FRR in the experiment.

Test	FRR: Experiment	FRR: Model	FRR: Model deviation
Fire test with HRR=165 kW	8 min 3 s [70]	9 min 18 s	15.5%

It should be noted that the CFRP load-bearing fraction increased from initial 0.44 to 0.49, by the time of coming in contact with decomposition front. The CFRP jacket fraction was dynamically corrected throughout the simulation as the predicted internal pressure grew. By the end of the test, to reach the load-bearing thickness, the decomposition front travelled the remaining safety margin fraction 1-0.49=0.51 (instead of initial 0.56).

5.3. Effect of degradation temperature on fire resistance rating

As the time to failure predicted by the model with CFRP decomposition temperatures 643-652 K was over-estimated by 15.5%, the effect from reduction of decomposition temperatures was investigated. Another fire test simulation implementing the lower decomposition temperatures, i.e. 613-633 K, was performed. The identified place of the tank failure was also in the dome location. The estimated time to tank failure totalled 7 min and 16 s. The temperature on the load-bearing thickness changing dynamically is shown in Figure 11.

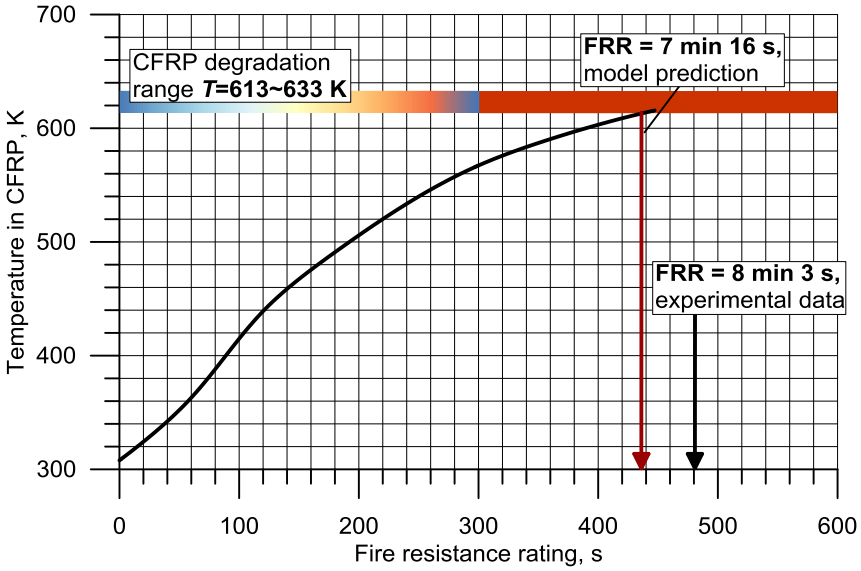

Figure 11. Visualisation of temperature history on the dynamically changing load bearing thickness of the tank CFRP jacket and its coincidence with decomposition wave temperatures 613-633 K.

The shown time to failure of the tank with CFRP decomposition wave 613-633 K and the result of previous numerical test are compared with experiment in Table 4.

Table 4. Comparison of the tank FRR predicted by model and FRR in the experiment.

Numerial fire test	FRR: Experiment	FRR: Model	FRR: Model deviation
CFRP with T_d=643~652 K	8 min 3 s [70]	9 min 18 s	+15.5%*
CFRP with T_d=613~633 K		7 min 16 s	-9.7%

Note: * - the symbols "+" and "-" before the deviation values mean over- and under-prediction respectively.

The numerical fire test with the lower decomposition temperatures (613-633 K) under-predicted the experiment with an error 9.7%. This result should be selected as representive in the current study for the reason of conservatism.

6.0 CONCLUSIONS

The novel 3D model for conjugate heat transfer from a fire to compressed gas storage vessel was developed and validated against the well-instrumented experiment performed at KIT. The test was performed with Type IV 70 MPa hydrogen storage tank subject to a 165 kW fire. The model included the original failure mechanism accounting for decomposition of the structural layer of the compressed gas storage tank in a fire and the internal gas pressure variation. In this study, the 3D model demonstrated the exact determination of the tank failure location and the time to failure, i.e. fire resistance rating.

The importance of 3D modelling is highlighted, as it allowed for revealing of the most vulnerable to a fire regions of the tank, i.e. dome parts of the structural composite jacket. It was shown that the tank composite layer degradation in a fire was non-uniform, as the thermal aggression was specific to the fire source design and the flame shielding. This precise analysis would be impossible with such simplifications as 1D or 2D modelling.

The model showed the complex prediction of several experimental parameters, such as temperatures and pressures, with an acceptable engineering accuracy. The temperatures of the flame above the burners deviated from experimental within 12%; the temperatures in the facility above the tank were reproduced with the maximum 8% deviations and the side temperatures (2 m away from the tank) were reproduced

with the maximum 12% deviations. The pressures inside the tank and inside the testing facility were reproduced with 1% and 20% overprediction respectively.

The FRR (time to failure) of the tank was reproduced using the original failure mechanism which is a part of the model. The predicted FRR totalled 9 min 18 s which is an over-estimation by 1 min 15 s (15.5%) compared to the experimental FRR (8 min 3 s). The selected decomposition temperature range implemented in the failure mechanism was 643-652 K. The parametric study of effect of resin decomposition temperatures on FRR was performed after. It was demonstrated that with the lower temperatures (613-633 K) the conservative FRR was achieved, i.e. 7 min 16 s, which under-predicts the experiment by 47 s (9.7%).

The 3D modelling of the Type IV tank in a fire revealed that the structural jacket has the vulnerable to thermal aggression areas (domes), as the thickness vary in different parts of the tank, e.g. cylindrical part is thicker than domes by about 44%. The composite thickness in the cylindrical part is 28 mm whereas the dome's thickness is ~22 mm. The tank failure in a fire shall be mostly attributed to the thinnest tank wall location (the domes) as the degradation front propagating inside thinner walls will cause the failure of the tank sooner in these locations, than in the cylindrical part. Following this observation, the authors suggest the safety strategy for the composite pressure vessels that will imply strengthening of the composite structural overwrap in the dome parts, i.e. equalisation of the jacket thickness. This will increase the fire resistance of compressed gas storage vessels.

7.0 ACKNOWLEDGEMENTS

The authors are grateful to the Engineering and Physical Sciences Research Council (UK) for funding the study through The Hydrogen and Fuel Cells Supergen Hub project (EP/J016454/1 and EP/P024807/1); SUPERGEN Challenge "Integrated safety strategies for onboard hydrogen storage" (EP/K021109/1); "Novel Education and Training Tools based on digital applications related to Hydrogen and Fuel Cell Technology" (NET-Tools) (No. 736648).

Thanks to Dr Farid Arya from Ulster University (UK) for the measurement of CFRP material properties and to Dr Yangkyun Kim from Korea Institute of Civil Engineering and Building Technology (South Korea) for performing TGA experiments with CFRP. Special thanks to our colleagues at Karlsruhe Institute of Technology (Germany), including but not limited to Dr Andreas Friedrich and Prof Thomas Jordan. Also thanks to Mr Per Heggem from Hexagon Composites (Norway).

REFERENCES

[1] Hawkes, 'US – CNG Tank Explodes on Garbage Truck', *Hawkesfire*, 12-Feb-2016. [Online]. Available: http://www.hawkesfire.co.uk/36706. [Accessed: 12-Jan-2016].

[2] YouTube, 'Car explosion in gas station', 2013. [Online]. Available: https://www.youtube.com/watch?v=wPHfiwPSDPM. [Accessed: 01-Dec-2016].

[3] YouTube/Disaster Channel, 'St. Louis Gas Cylinders Disaster', *YouTube*. [Online]. Available: https://www.youtube.com/watch?v=EPuTQYHnfoc. [Accessed: 01-Dec-2016].

[4] YouTube, 'Must See - Power of Liquid Natural Gas Explosion Accident - Incredible Footage - China', *YouTube*. [Online]. Available: https://www.youtube.com/watch?v=UI0QWm4TxZU. [Accessed: 01-Dec-2016].

[5] A. Shaukat, 'Transport safety: CNG cylinders killed more people than US drones: Report', *The Express Tribune*, 2012. [Online]. Available: http://tribune.com.pk/story/362282/transport-safety-cng-cylinders-killed-more-people-than-us-drones-report/. [Accessed: 01-Dec-2016].

[6] M. Dadashzadeh, S. Kashkarov, D. Makarov, and V. Molkov, 'Socio-economic effects of safety measures on hydrogen-powered vehicles in UK', presented at the International Conference on Hydrogen Safety (ICHS) 2017, (SUBMITTED), 2017.

[7] S. Kashkarov, Z. Li, and V. Molkov, 'Nomograms for assessment of hazard distances from a blast wave after high-pressure hydrogen cylinder rupture in a fire', presented at the Eighth International Seminar on Fire & Explosion Hazards (ISFEH8), Hefei, China, 2016.

[8] V. Molkov and S. Kashkarov, ‘Blast wave from a high-pressure gas tank rupture in a fire: stand-alone and under-vehicle hydrogen tanks’, *International Journal of Hydrogen Energy*, vol. 40, no. 36, pp. 12581–12603, 2015.
[9] V. Shentsov, W. Kim, D. Makarov, and V. Molkov, ‘Numerical simulations of experimental fireball and blast wave from a high-pressure tank rupture in a fire’, presented at the Proc. of the Eighth International Seminar on Fire & Explosion Hazards (ISFEH8), Hefei, China, 2016.
[10] V. Shentsov, D. M. C. Cirrone, D. Makarov, and V. Molkov, ‘Simulation of fireball and blast wave from a hydrogen tank rupture in a fire’, presented at the The International Symposium on Nonequilibrium Processes, Plasma, Combustion and Atmospheric Phenomena, Sochi, Russia, 2016, pp. 435–442.
[11] Department for Communities and Local Government, ‘Fire Statistics Great Britain 2011/12’. [Online]. Available: https://data.gov.uk/dataset/vehicle_fires.
[12] NFPA, ‘U.S. vehicle fire trends and patterns’. 2010.
[13] B. Evarts, ‘Fires at U.S. Service Stations’, NFPA, 2011.
[14] Department for Communities and Local Government, ‘Fire spread in car parks, BD2552’. BRE, 2010.
[15] Z. Saldi and J. X. Wen, ‘Modeling thermal response of polymer composite hydrogen cylinders subjected to external fires’, presented at the ICHS 2015, Yokohama, Japan, 2015.
[16] N. Weyandt, ‘Analysis of Induced Catastrophic Failure Of A 5000 psig Type IV Hydrogen Cylinder’, Southwest Research Institute report for the Motor Vehicle Fire Research Institute, 01.06939.01.001, 2005.
[17] J. Hu, J. Chen, S. Sundararaman, K. Chandrashekhara, and W. Chernikoff, ‘Analysis of composite hydrogen storage cylinders subjected to localized flame impingements’, *International Journal of Hydrogen Energy*, vol. 33, pp. 2738–2746, 2008.
[18] J. Zheng *et al.*, ‘Experimental and numerical studies on the bonfire test of high-pressure hydrogen storage vessels’, *Int. J. Hydrog. Energy*, vol. 35, no. 15, pp. 8191–8198, 2010.
[19] J. Zheng *et al.*, ‘Experimental and numerical investigation of localized fire test for high-pressure hydrogen storage tanks’, *Int. J. Hydrog. Energy*, vol. 38, no. 25, pp. 10963–10970, 21 2013.
[20] J. Zheng *et al.*, ‘Heat transfer analysis of high-pressure hydrogen storage tanks subjected to localized fire’, *Int. J. Hydrog. Energy*, vol. 37, no. 17, pp. 13125–13131, 2012.
[21] D. Halm and T. Van Eekelen, ‘WP5 - Modelling part. Simulation of the mechanical behaviour of composite pressure vessels subjected to fire’, 2016.
[22] J. B. Henderson, J. A. Wiebelt, and M. R. Tant, ‘A model for thermal response of polymer composite materials with experimental verification’, *Journal of Composite Materials*, vol. 19, pp. 579–595, 1985.
[23] R. M. Sullivan, ‘A coupled solution method for predicting the thermostructural response of decomposing, expanding polymeric composites’, *Journal of Composite Materials*, pp. 408–434, 1993.
[24] H. L. McManus and G. S. Springer, ‘High temperature behaviour of thermomechanical behaviour of carbon-phenolic and carbon-carbon composites’, *Journal of Composite Materials*, vol. 26, pp. 206–229, 1992.
[25] A. G. Gibson, Y. S. Wu, H. W. Chandler, J. A. D. Wilcox, and P. Bettess, ‘A model for the thermal performance of thick composite laminates in hydrocarbon fires’, *Rev. L’Inst Franc Petrol*, no. 50, pp. 69–74, 1995.
[26] Y. I. Dimitrienko, ‘Thermomechanical behaviour of composite materials and structures under high temperatures: 1. Materials’, *Composites Part A: Applied Science and Manufacturing*, vol. 28, no. 5, pp. 453–461, 1997.
[27] L. Bustamante Valencia, P. Blanc-Vannet, L. Heudier, and D. Jamois, ‘Thermal history resulting in the failure of lightweight fully-wrapped composite pressure vessel for hydrogen in a fire experimental facility’, *Fire Technology*, no. 52, pp. 421–442, 2016.
[28] United Nations Economic Commission for Europe, ‘Global technical regulation on hydrogen and fuel cell vehicles. Addendum 13: Global technical regulation No. 13. Global Registry.’, UNECE, Global Registry, 2013.
[29] A. Friedrich, ‘Private communication’, 2015.

[30] A. Friedrich, G. Stern, and G. Necker, ‘TA project 2038 “R&D of high pressure hydrogen storage system with increased fire resistance rating”’, presented at the H2FC-European Technical School on Hydrogen and Fuel Cells 2015, Greece, 2015.
[31] B. E. Launder and D. B. Spalding, *Lectures in Mathematical Models of Turbulence*. London, England: Academic Press, 1972.
[32] B. F. Magnussen and B. H. Hjertager, ‘On mathematical models of turbulent combustion with special emphasis on soot formation and combustion’, in *16th Symp. (Int’l.) on Combustion*, The Combustion Institute, 1976.
[33] E. H. Chui and G. D. Raithby, ‘Computation of radiant heat transfer on a nonorthogonal mesh using the finite-volume method’, *Numerical Heat Transfer*, vol. 23, no. Part B, pp. 269–288, 1993.
[34] G. D. Raithby and E. H. Chui, ‘A Finite-Volume Method for Predicting a Radiant Heat Transfer in Enclosures with Participating Media’, *Journal of Heat Transfer*, vol. 112, pp. 415–423, 1990.
[35] R. Siegel and J. R. Howell, *Thermal Radiation Hear Transfer*, 2nd ed. New York, London: McGraw-Hill, 1981.
[36] H. C. Hottel and A. F. Sarofim, *Radiative transfer*. New York: McGraw-Hill Book Company, 1967.
[37] T. F. Smith, Z. F. Shen, and J. N. Friedman, ‘Evaluation of coefficients for the weighted sum of grey gases model’, *Journal of Heat Transfer*, vol. 104, pp. 602–608, 1982.
[38] SAS IP, Inc., *ANSYS Fluent*. 2016.
[39] O. Redlich and J. N. S. Kwong, ‘On the thermodynamics of solutions. V. An equation of state. Fugacities of gaseous solutions’, vol. 44, no. 1, pp. 233–244, 1949.
[40] P. Heggem, ‘Private communication’, 2013.
[41] S. Welch, R. Hadden, J. Hidalgo-Medina, and P. Pironi, ‘WP3 Thermal properties of composite materials exposed to fire’, presented at the FireComp project webinar, Paris, 2016.
[42] F. Cverna, ASM Ready Reference: Thermal properties of metals. ASM International, 2002.
[43] Y. Toulouevski and I. Zinurov, Innovation in Electric Arc Furnaces: Scientific Basis for Selection, 2nd ed. Springer, 2014.
[44] M. W. Pilling, B. Yates, M. A. Black, and P. Tattersall, ‘The thermal conductivity of carbon fibre-reinforced composites’, *Journal of Material Science*, vol. 14, pp. 1326–1338, 1979.
[45] R. C. Wetherhold and J. Wang, ‘Difficulties in the theories for predicting transverse thermal conductivity of continuous fiber composites’, vol. 28, no. 15, pp. 1491–1498, 1994.
[46] A. Dasqupta and R. K. Agarwal, ‘Orthotropic thermal conductivity of plain-weave fabric composites using a homogenization technique’, *Journal of Composite Materials*, vol. 26, pp. 2736–2758, 1992.
[47] D. Quang Dao, J. Luche, F. Richard, T. Rogaume, C. Bourhy-Weber, and S. Ruban, ‘Determination of characteristic parameters for the thermal decomposition of epoxy resin/carbon fibre composites in cone calorimeter’, vol. 38, pp. 8167–8178, 2013.
[48] J. P. Hidalgo, P. Pironi, R. M. Hadden, and S. Welsh, ‘Effect of thickness on the ignition behaviour of carbon fibre composite materials used in high pressure vessels’, presented at the Proc. of the Eighth International Seminar on Fire & Explosion Hazards (ISFEH8), Hefei, China, 2016, vol. (SUBMITTED).
[49] T .Tian and K. D. Kole, ‘Anisotropic thermal conductivity measurement of carbon-fiber/epoxy composite materials’, *International Journal of Heat and Mass Transfer*, vol. 55, pp. 6530–6537, 2012.
[50] R. D. Sweeting, ‘Measurement of thermal conductivity for fibre-reinforced composites’, *Composites Part A: Applied Science and Manufacturing*, vol. 35, pp. 933–938, 2004.
[51] J. Liang, M. Saha, and M. C. Altan, ‘Effect of carbon nanofibers on thermal conductivity of carbon fiber reinforced composites’, *Procedia Engineering*, vol. 56, pp. 814–820, 2013.
[52] C. T. Pan and H. Hocheng, ‘Evaluation of anisotropic thermal conductivity for unidirectional FRP in laser machining’, vol. 32, pp. 1657–1667, 2001.
[53] ASM International, *Engineered materials handbook*, vol. 1 Composites. Metals Park, OH, 1987.
[54] M. Monde and M. Kosaka, ‘Understanding of thermal characteristics of fueling hydrogen high pressure tanks and governing parameters’, *SAE Int. J. Alt. Power.*, pp. 61–67, 2013.
[55] J. H. Lee, ‘Thermal decomposition kinetics and heat transfer mechanism of carbon fiber reinforced plastic applied in a fuel storage vessel’. The University of Seoul, 2012.

[56] Mitsubishi Plastics, ‘Comparison table of properties of various materials’, 2015. [Online]. Available: https://www.mpi.co.jp/english/products/industrial_materials/pitch_based_carbon_fiber/pbcf003.html#anc04. [Accessed: 11-Mar-2015].
[57] F. Arya, ‘Private communication’, 2016.
[58] M. A. Starnes, N. J. Carino, and E. A. Kausel, ‘Preliminary Thermography Studies for Quality Control of Concrete Structures Strengthened with Fiber-Reinforced Polymer Composites’, in *Journal of Materials in Civil Engineering*, 2003, pp. 266–273.
[59] G. Wang, J. Zhou, S. Hu, S. Dong, and P. Wei, ‘Investigations of filling mass with the dependence of heat transfer during fast filling of hydrogen cylinders’, *International Journal of Hydrogen Energy*, vol. 39, pp. 4380–4388, 2014.
[60] J. Meyer, ‘Optimisation of onboard hydrogen storage fire resistance’, Ulster University, UK, 2012.
[61] ‘Idemat Database’, Delft University of Technology, 2003.
[62] W. Liu, R. J. Varley, and G. P. Simon, ‘Understanding the decomposition and fire performance processes in phosphorus and nanomodified high performance epoxy resins and composites’, vol. 48, pp. 2345–2354, 2007.
[63] J. L. Merino-Pérez, A. Hodzic, E. Merson, and S. Ayvar-Soberanis, ‘On the temperatures developed in CFRP drilling using uncoated WC-Co tools Part II: Nanomechanical study of thermally aged CFRP composites’, vol. 123, pp. 30–34, 2015.
[64] N. Régnier and S. Fontaine, ‘Determination of the thermal degradation kinetic parameters of carbon fibre reinforced epoxy using TG’, vol. 64, pp. 789–799, 2001.
[65] PerkinElmer Inc, ‘Characterization of Polymers Using TGA’. [Online]. Available: http://www.perkinelmer.com/CMSResources/Images/44-132088APP_CharacterizationofPolymersUsingTGA.pdf. [Accessed: 24-Apr-2015].
[66] T. Niranjana Prabhu, Y. J. Hemalatha, V. Harish, K. Prashantha, and P. Iyengar, ‘Thermal Degradation of Epoxy Resin Reinforcedwith Polypropylene Fibers’, *Wiley InterScience*, 2006. [Online]. Available: www.interscience.wiley.com. [Accessed: 24-Apr-2015].
[67] C.-L. Chiang, R.-C. Chang, and Y.-C. Chiu, ‘Thermal stability and degradation kinetics of novel organic/inorganic epoxy hybrid containing nitrogen/silicon/phosphorus by sol–gel method’, vol. 453, pp. 97–104, 2007.
[68] Y. Kim, ‘Private communication’, 2016.
[69] R. E. Lyon and J. G. Quintiere, ‘Criteria for piloted ignition of combustible solids’, *Combustion and Flame*, vol. 151, pp. 551–559, 2007.
[70] D. Makarov, Y. Kim, S. Kashkarov, and V. Molkov, ‘Thermal protection and fire resistance of high-pressure hydrogen storage’, presented at the Eighth International Seminar on Fire & Explosion Hazards (ISFEH8), Hefei, China, 2016.